JOURNAL OF AIRCRAFT
Vol. 31, No. 6, November–December 1994

Unstructured Grid Solutions to a Wing/Pylon/Store Configuration

Paresh Parikh* and Shahyar Pirzadeh†
ViGYAN, Inc., Hampton, Virginia 23666
and
Neal T. Frink‡
NASA Langley Research Center, Hampton, Virginia 23681

The purpose of this article is to validate an inviscid flow solution package based on a new unstructured grid methodology using experimental data on a wing/pylon/finned store configuration. The solution package consists of an advancing front grid generator, VGRID, and an efficient Euler equation solver, USM3D. Comparisons of computed data vs experimental data are made for two freestream Mach numbers at five store locations relative to the wing. Both rigid body aerodynamics and mutual interference effects are explored. A very good agreement is observed between computed and wind-tunnel data.

Introduction

A GOOD understanding of physics in carriage and release of stores from an aircraft is of primary interest to the aircraft designer. The forces and moments acting on the airframe have not only a performance impact on the mission, but also a safety impact on the aircraft. The flowfield encountered on stores (missiles, bombs, external fuel tanks, etc.) in the presence of an aircraft is usually very complex due to mutual interference of multiple bodies. Traditionally, the designers have resorted to wind tunnels to estimate interference aerodynamics. However, recent years have seen an emergence of the application of computational fluid dynamic (CFD) techniques to the store separation problem. Both multiblocked structured and overlapping grid methods have been successfully used to solve multibody problems.[1-4] Although very efficient multiblocked flow solvers are available, the grid generation currently requires a considerable amount of time. For the chimera overlapping scheme, on the other hand, the grid generation is a relatively simple task, but the flow solver tends to be more sophisticated because of a large amount of bookkeeping required for interpolation between component grids.

The use of unstructured grids has grown considerably in recent years due to their ability to produce quality grids around complex configurations with ease. The technology for generating grids and solving the inviscid fluid flow equations on unstructured grids has matured to the point that it is being applied more routinely for computing solutions over complex configurations.[5-10] This inherent flexibility of unstructured grids makes the methodology a good candidate for the analysis of flow around a multibodied configuration.

In this article the flowfield about a wing/pylon/store configuration is analyzed using a new unstructured grid, Euler analysis package. The package consists of an unstructured tetrahedral grid generator VGRID, and an Euler equation solver USM3D. The grid generator is an interactive, tetrahedral unstructured grid generator based on the advancing-front technique.[11] A version with restart capability and a postprocessing option has been in use among the research community for some time now.[12] The flow solver is an upwind, cell-centered, finite-volume Euler solver for the unstructured tetrahedral grids. Over the past few years, both of these programs have been successfully applied to several complex three-dimensional configurations.[9,10] In the following sections the grid generation procedure is described, followed by details of the flow solver. Finally, results computed at two Mach numbers and for several store positions are presented, compared, and analyzed.

Configuration Geometry and Data Base

The present investigation is conducted for a wing/pylon/finned-store configuration reported in Ref. 13. The configuration consists of a clipped delta wing with a 45-deg sweep comprised from a constant NACA 64A010 symmetrical airfoil section. The wing has a root chord of 15 in., a semispan of 13 in., and a taper ratio of 0.134. The pylon is located at midspan station and has a cross section that is characterized by a flat plate closed at the leading and trailing edges by a symmetrical ogive shape. The width of the pylon is 0.294 in. The four fins on the store are defined by a constant NACA 0008 airfoil section with a leading-edge sweep of 45 deg and a truncated tip. All the available wind-tunnel data had cylindrical stings attached to the wing and store. However, since the computational geometry available did not have these stings, they were not modeled for the calculations reported here. A schematic of the configuration is shown in Fig. 1, whereas a cross section at the wing-pylon junction station is shown in Fig. 2.

In Ref. 13 an extensive data base has been reported for two Mach numbers of 0.95 and 1.20, including steady-state pressure distributions on all the components, as well as both steady-state and transient forces and moments data on the store. The steady-state data are available for the store-in-carriage and for several other store locations. For this study, steady-state computations were performed for both Mach numbers corresponding to selected store positions shown in Tables 1 and 2. These store positions are representative of the carriage position (baseline), an intermediate position (near), and the farthest position (far). The corresponding run numbers from the experimental data are provided in the following tables for reference. Note that the dropped positions in Tables

---

Received Aug. 5, 1992; revision received Nov. 12, 1993; accepted for publication Feb. 20, 1994.

*Vice President. Senior Member AIAA.

†Research Engineer. Member AIAA.

‡Senior Research Engineer. Senior Member AIAA.

Table 1 Store data for $M_\infty = 0.95$ cases

		Store translations			Store rotations		
	Store position	ΔX, in.	ΔY, in.	ΔZ, in.	Ψ, deg, yaw	Θ, deg, pitch	Φ, deg, roll
Run 1	Baseline	0.00	0.00	0.00	0.00	0.00	0.00
Run 8	Near	0.21	−0.17	−1.78	4.95	5.20	2.80
Run 10	Far	0.78	−0.31	−3.98	12.01	2.27	6.30

Table 2 Store data for $M_\infty = 1.20$ cases

		Store translations			Store rotations		
	Store position	ΔX, in.	ΔY, in.	ΔZ, in.	Ψ, deg, yaw	Θ, deg, pitch	Φ, deg, roll
Run 4	Baseline	0.00	0.00	0.00	0.00	0.00	0.00
Run 12	Near	0.19	−0.08	−1.68	3.10	5.18	1.70
Run 14	Far	1.00	−0.09	−5.05	9.41	1.09	6.50

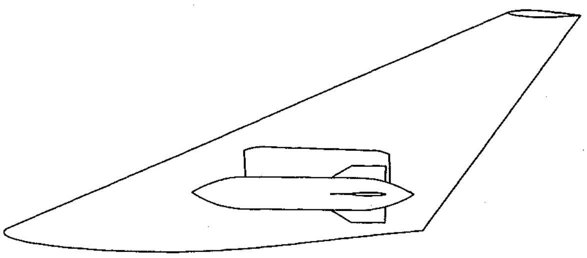

Fig. 1 Schematic of the wing/pylon/store configuration.

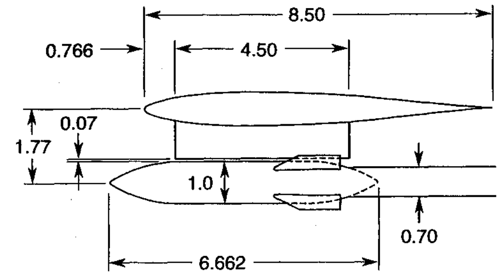

Fig. 2 Cross-section of the configuration at wing-pylon junction (all dimensions are in inches).

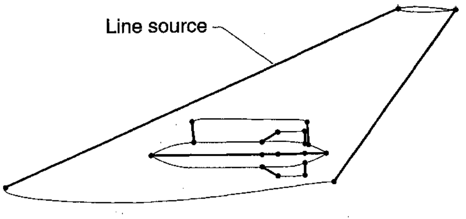

Fig. 3 Locations of linear source elements for grid spacing control.

1 and 2 are different for the two Mach numbers. The translations ΔX, ΔY, and ΔZ are referenced to the store c.g. that is located 2.79 store diam aft of its nose along the cylindrical axis. The orientation of the coordinate system in the tables is X positive downstream, Y positive spanwise, and Z positive up. The rotations Ψ, Θ, and Φ are positive with yaw outboard, pitch nose up, and roll outboard, respectively. The store rotations were obtained by standard Euler transformations about the store c.g.

Grid Generator VGRID

The computational grids were generated using a version of VGRID that has been modified to utilize a new "structured background" grid concept.[14] In most advancing-front grid generators, the grid element size is controlled by grid spacing parameters specified at the nodes of a secondary coarse grid called the "background grid." In the conventional method (e.g., Ref. 11), the background grid consists of a number of tetrahedral cells that completely encloses the domain to be gridded. The smoothness of the final grid depends upon the smoothness in the variation of grid spacings prescribed at the background grid nodes manually. For this reason, the conventional method requires considerable user interaction to produce desired smoothness in the surface and field grid. In the new method, a smooth grid element size variation is achieved by solving an elliptic partial differential equation on a uniform Cartesian background grid. The desired distribution of grid spacing parameters in the field is obtained by specifying a number of "point" and "line" sources, and solving a Poisson equation on the Cartesian grid. The approach is analogous to modeling the diffusion of heat from discrete heat sources in a conducting medium. In addition to symmetrical propagation of grid spacings, the new method is capable of controlling the directional propagation of the sources. This method of grid generation has been successfully applied to several two-dimensional and simple three-dimensional configurations.[12,14] However, this was its first full application to a complex three-dimensional geometry. In addition to an improved grid quality, the new method has reduced the grid generation times considerably.

For all computations, the outer boundaries were located at 6 root chord lengths (6C) ahead, above, and below the wing, and 10C behind the wing trailing edge. In the spanwise direction, the outer boundary was 2.5C away from the symmetry plane. For all the cases, a 29 × 23 × 7 background grid was used. The grid spacings were controlled using 8 point and 13 line sources. The positions of line sources are shown in Fig. 3. The line source positioned along the axis of the store propagates symmetrically, while the line sources along the leading and trailing edges of the wing, pylon, and fins have directional intensity control. The eight point sources were placed at the corners of the outer computational boundaries.

A single surface mesh was generated and maintained for all subsequent volume grids. This surface triangulation consisted of 13,526 points and 27,044 triangles, including the grid on the plane of symmetry and outer computational boundaries. Figure 4a shows surface triangulation on the whole configuration. In Fig. 4b, a close-up of the fin area is shown. As can be seen, a smooth grid distribution on the surface and a convenient control over grid resolution in regions such as the leading edges of the wing and fins is obtained.

The baseline configurations with the store in the carriage position (runs 1 and 4) contained a small gap ($\Delta Z = 0.07$ store diam) between the store and pylon. Before generating the volume grid, the store was moved down another 0.1 store diam, opening the gap further to ensure that several layers of cells were placed in the gap. A volume grid was generated during several restart runs. Once the volume grid generation

Table 3 Grid sizes for M_∞ = 0.95 cases

	Store position	Total cells	Total points
Run 1	Baseline	567,862	103,064
Run 8	Near	463,093	85,439
Run 10	Far	427,991	79,464

Table 4 Grid sizes for M_∞ = 1.20 cases

	Store position	Total cells	Total points
Run 4	Baseline	567,862	103,064
Run 12	Near	700,261	125,921
Run 14	Far	683,348	121,200

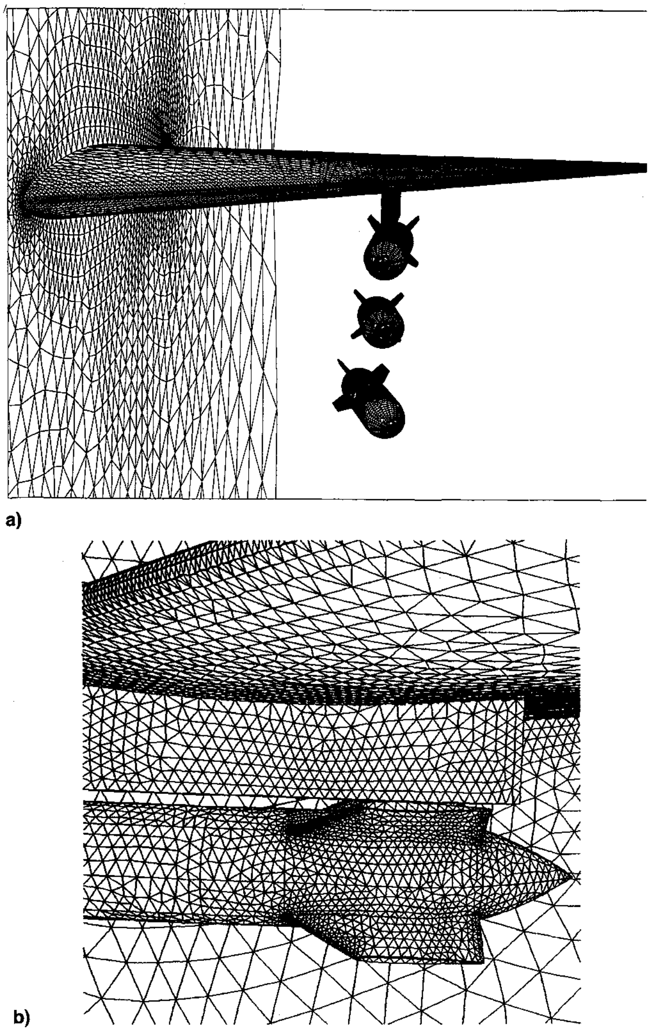

Fig. 4 a) Surface triangulation on the wing/pylon/store configuration and b) close-up view of surface grid near fins.

was completed, the store was moved back to the correct position, and the volume grid points adjusted using a grid moving technique based on the "spring system" analogy. Finally, the quality of the volume grid was improved through a postprocessing operation during which most of the distorted cells were identified, removed, and regenerated.

The volume grids for the remaining cases (runs 8, 10, 12, and 14) were generated using the same surface mesh, but with the store surface grid and sources repositioned according to the translations and rotations prescribed in Tables 1 and 2. The strength and intensity of source elements were adjusted to obtain the desired volume grid distributions for each case. The resulting grid sizes for each case are listed in Table 3 for Mach number 0.95 and in Table 4 for Mach number 1.2. The entire process of grid generation for the baseline grid, which included construction of surface patches, preparation and adjustment of background grid, generation of the surface and volume grid, and postprocessing the grid, took about 4 days. The time required for generating each subsequent grid was on the order of several hours.

Flow Solver USM3D

The flow solutions were computed with an efficient Euler equation solver for unstructured tetrahedral cells.[8-10] In this method, the spatial discretization is accomplished by a cell-centered finite-volume formulation using Roe's flux-difference splitting. A novel cell reconstruction process, which is based on an analytical formulation for computing solution gradients within tetrahedral cells, is used for the higher-order differencing. Solutions are advanced in time by a three-stage Runge-Kutta time-stepping scheme with convergence accelerated to steady state by local time stepping and implicit residual smoothing. The code requires 17.5 μ-s/cell/iteration on a Cray Y-MP with a core memory requirement of about 45 words/cell. For the present calculations this translated to between 19.5–31.6 Mwords of core memory.

Boundary Conditions

A flow tangency condition was imposed on the wing and center plane by setting the velocities on the boundary faces to their cell-center values and then subtracting the component normal to the solid surface. Density and pressure boundary conditions were simply set to the cell-centered value.

Characteristic boundary conditions were applied to the far-field boundary for each computation using the fixed and extrapolated Riemann invariants corresponding to the incoming and outgoing waves. The incoming Riemann invariant is determined from the freestream flow, and the outgoing invariant is extrapolated from the interior domain. The invariants are used to determine the locally normal velocity component and speed of sound. At an outflow boundary, the two tangential velocity components and the entropy were extrapolated from the interior, while at the inflow boundary they were specified as having far-field values. These five quantities provide a complete definition of the flow in the far field.

Results

This section presents results obtained for all the cases mentioned earlier. Since the primary aim of this article is to validate the solution package, for the most part the results are presented in the form of C_p distributions. Some surface contour plots and force data comparisons are also presented. In the interest of brevity only representative results are presented here, the reader is referred to Ref. 15 for detailed results. In this section the results are presented under two subsections, one for each Mach number.

Surface Pressures for M_∞ = 0.95

The first case studied compares results for three runs at M_∞ = 0.95, and a wing angle of attack equal to 0.0 deg. Besides the baseline (or store-in-carriage) position (run 1), a store "near" (run 8) and a store "far" (run 10) positions were selected from Ref. 13. The converged flow solutions for all the three runs were obtained with a Courant-Friedrichs-Lewy (CFL) number of 4 in about 2000 iterations, while the L_2 norm (rms average of all residuals) decreased to about 4 orders of magnitude. For the baseline position, the computation required about 5.7 h of Cray Y-MP time, whereas for the other two positions, the required computational time was of the order of 4.0 CPU h.

Detailed pressure comparisons are shown in the next three figures. Figure 5 compares computed and experimental data on the wing at a spanwise station corresponding to 1.2 store diam inboard of the pylon for all three store positions. For all cases, comparison with experimental data is excellent on

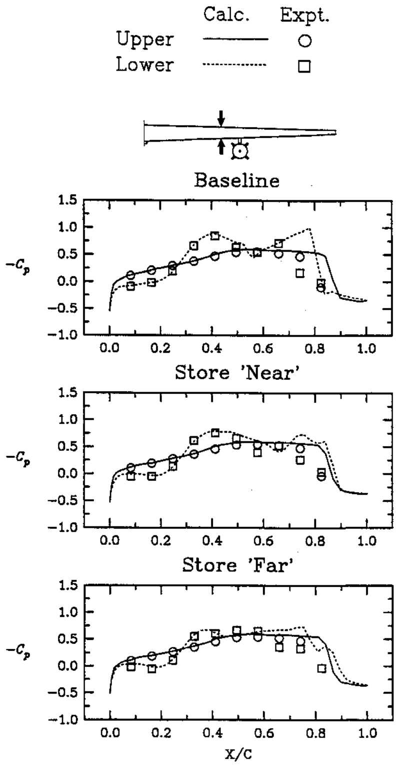

Fig. 5 Surface pressure comparison on the wing at 1.2 store diam inboard of pylon location, $M_\infty = 0.95$.

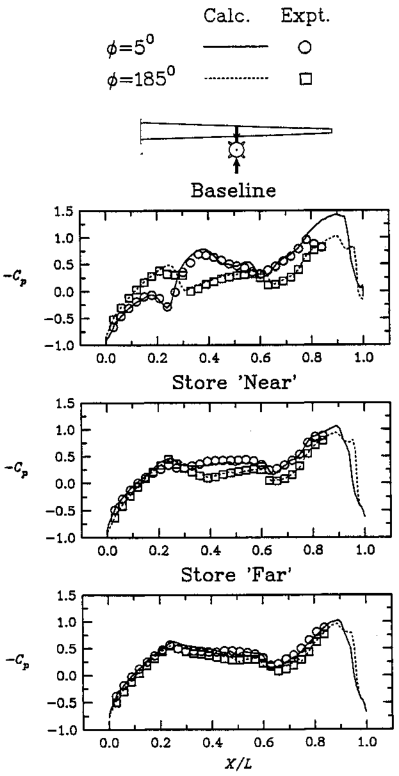

Fig. 6 Surface pressure comparison on the store along streamwise rays, $M_\infty = 0.95$.

both the upper and the lower surface up to about 70% chord. As expected from a Euler solution, the computations predict a shock location that is downstream of that measured by the experiments. The pressure distribution on the upper surface is similar for all cases, showing essentially no interference effect from the store, although on the lower surface the interference effect is the strongest for the baseline position and reduces as the store moves farther away.

For the store, the results are compared along streamwise rays from the nose to the tail. The location for each ray is identified by the circumferential angle ϕ, which is defined positive clockwise from the pylon center looking downstream. In Fig. 6, data is presented at rays along the top and bottom of the store at $\phi = 5$ and 185 deg, respectively. For all cases, the computed pressure coefficient compares very well with experimental data. In particular, the reader's attention is drawn to the comparison along the 5-deg ray for the baseline configuration that passes through the gap between the store and the pylon and where a large interference is expected.

In Fig. 7, comparison with the experimental data is shown on all the fins for the "baseline" configuration. The chordwise pressure distribution is plotted at approximately midspan for each fin. The "left" and "right" in this figure refer to the observer's left and right, respectively, when viewed from the store looking downstream. The overall agreement with the experimental data is good. As can be seen, fins 1 and 4 experience large interference as compared to fins 2 and 3 that are away from the underside of the wing.

Surface Pressures for $M_\infty = 1.20$

The next case is for the freestream condition of $M_\infty = 1.20$, and a wing angle of attack equal to 0.0 deg. The three store positions for which comparison with the experimental data is made correspond to runs 4 (baseline), 12 (store near), and 14 (store far). For the baseline position, the converged solution was obtained in 1125 iterations with a CFL number of 4, while the L_2-norm decreased to about 3.5 orders of magnitude in about 3 h of Cray Y-MP time. For the other two store positions, the calculations required 4.0 and 6.7 Cray Y-MP h, respectively, for a residual drop of 3 and 5 orders of magnitude, respectively. For this case, surface C_p contours are presented first, followed by comparison with experimental data. Figure 8 shows C_p contours on the wing lower surface for the baseline case, where a strong interference effect from the store and the pylon can be seen. The effect of the detached shock from the nose of the store and from the fins and the asymmetry due to the crossflow are evident. The horseshoe shock pattern behind the store is the footprint of a conical shock structure emanating from the aft apex of the store.

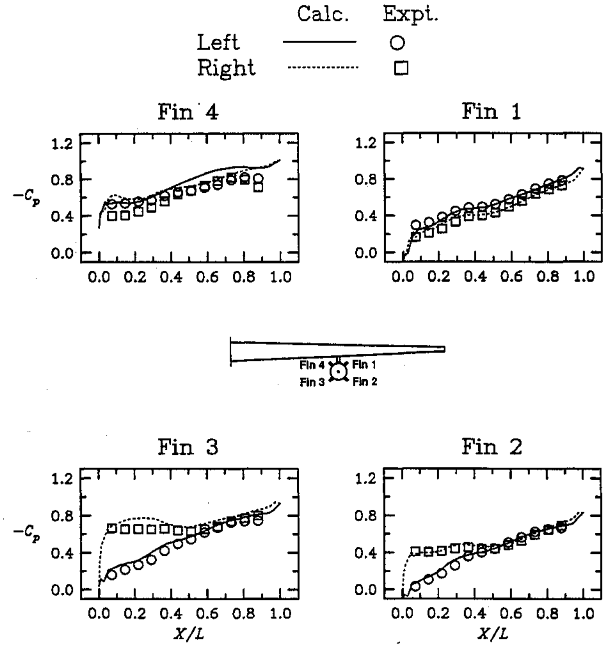

Fig. 7 Surface pressure comparison on the fins for the baseline configuration, $M_\infty = 0.95$.

For this case, the calculated pressures on the wing compare very well with the experimental data, indicating a reduction in interference as the store moves farther away from the wing,

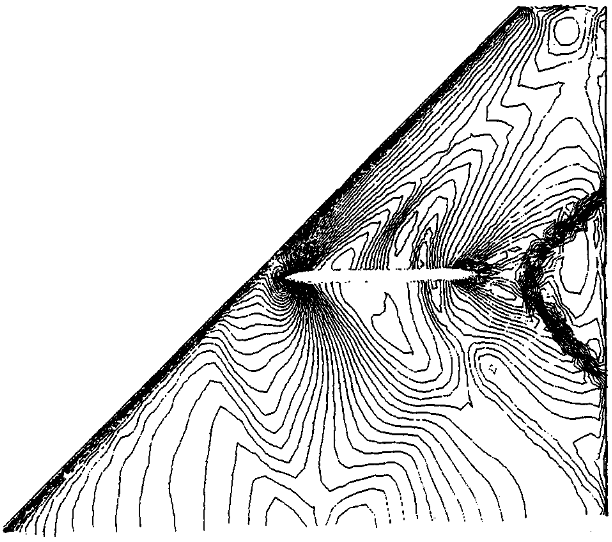

Fig. 8 C_p contours on the wing for the baseline configuration, M_∞ = 1.20.

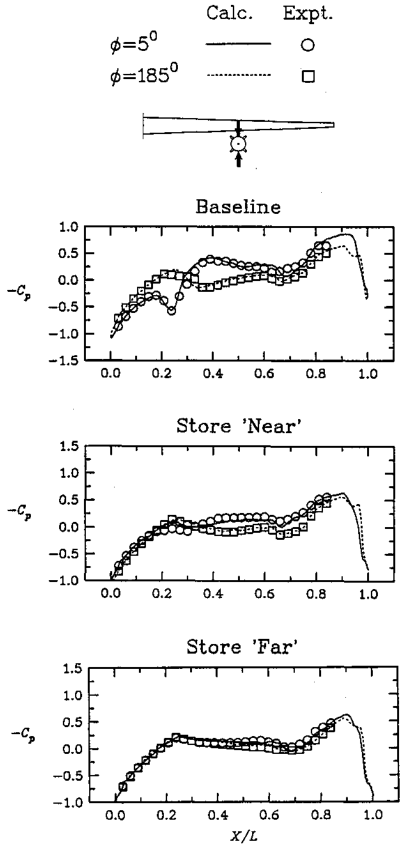

Fig. 9 Surface pressure comparison on the store along streamwise rays, M_∞ = 1.20.

similar to the transonic case. These results are, however, not shown in the interest of brevity. Interested readers are referred to Ref. 15.

Figure 9 depicts the store C_p distribution along rays at $\phi = 5$ and 185 deg, similar to the one for the transonic case shown in Fig. 6. Once again comparison with experimental data is excellent for all store positions.

Figure 10 shows comparison of pressure data on the fins for the store "near" case. In these figures, L and R refer to the observer's left and right side of the fin, respectively, when viewed from the store looking downstream. The agreement is very good for all four fins.

Table 5 Comparison of force and moment coefficients on the store

	M_∞ = 0.95		M_∞ = 1.20	
	Euler	Data	Euler	Data
C_N	0.687	0.644	0.537	0.520
C_Y	−1.036	−0.954	−0.540	−0.531
C_A	1.132	0.901	0.999	1.038
C_m	−1.761	−1.430	−1.631	−1.488
C_n	1.791	1.520	1.296	1.200
C_l	0.104	0.100	0.060	0.044

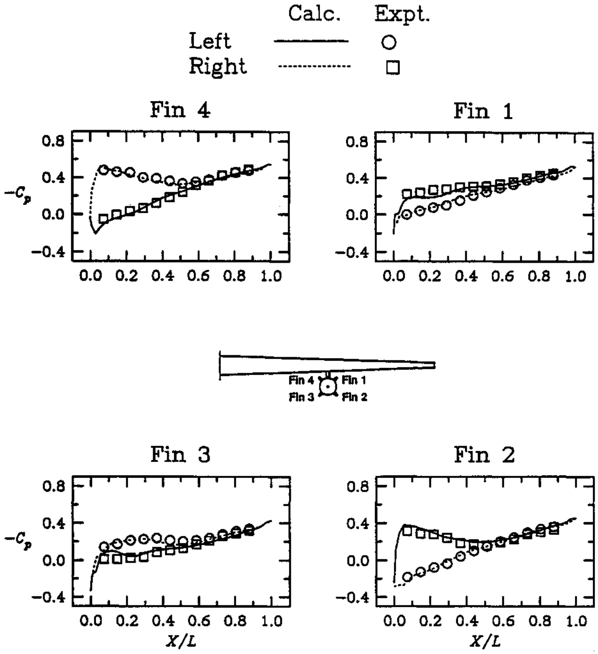

Fig. 10 Surface pressure comparison on the fins for the store near configuration, M_∞ = 1.20.

Forces and Moments

In addition to the pressure comparisons shown above, force and moment data were computed for several cases. Since the force and moment data for the store were measured under dynamic conditions, and since the current version of the flow solver did not have capability for the moving grids, the force and moment comparisons presented here are limited to the two steady-state store-in-carriage position runs (run 1 and 4). Results for the two cases are summarized in Table 5 in terms of force and moment coefficients. In Table 5 C_N, C_Y, and C_A are normal, side, and axial forces on the store, respectively, and C_m, C_n, and C_l are the pitching, yawing, and rolling moments, respectively. These coefficients are based on the store cross-sectional area, S_{ref} = 0.785 in.^{2} diam, d_{ref} = 1.0 in., and the c.g. that is located at 2.79 in. aft of the nose on the store centerline.

As can be seen, the comparison with experimental data is reasonable for the transonic case and very good for the supersonic case.

Conclusions

An inviscid flow solution package based on the unstructured grid has been validated using experimental data on a wing/pylon/store configuration. An emphasis has been placed on quantitative comparisons with experimental data in the form of C_p distributions.

The new version of the grid generator has resulted in a considerable reduction in grid generation times. Once the surface grid was generated for the baseline case, each of the subsequent volume grids were generated in a matter of hours using the restart capability of the grid generator. A new version of the flow solver, resulting from an improved data structure, has reduced the core memory and the CPU time requirements.

Computational results have been obtained at two Mach numbers of 0.95 and 1.2. For each Mach number, besides the baseline (or store-in-carriage) configuration, two other store locations relative to the wing have been analyzed. For all cases considered, a very close agreement (within the limitations of an inviscid solver) with the experimental data has been obtained. The pressure distributions on the mutually interfering bodies have been accurately estimated. The forces and moments on the store also compare favorably with the experimental data. The demonstrated accuracy and efficiency makes the package an attractive preliminary design/analysis tool.

Acknowledgments

The work of the first and second authors was supported by Transonic Aerodynamics Branch, NASA Langley Research Center under Contract NAS1-18585. The computations were carried out using Cray Y-MP at Central Scientific Computing Facility, NASA Langley Research Center, Hampton, Virginia, and at the Numerical Aerodynamic Simulation (NAS) facility at NASA Ames Research Center, Moffett Field, California.

References

[1] Lijewski, L. E., "Transonic Euler Solutions on Mutually Interfering Finned Bodies," *AIAA Journal*, Vol. 28, No. 6, 1990, pp. 982–988.

[2] Arabshahi, A., and Whitfield, D. L., "A Multi-Block Approach to Solving the Three-Dimensional Unsteady Euler Equations About a Wing-Pylon-Store Configuration," AIAA Paper 89-3401, Aug. 1989.

[3] Benek, J. A., Donegan, T. L., and Suhs, N. E., "Extended Chimera Grid Embedding Scheme with Application to Viscous Flows," AIAA Paper 87-1126, June 1987.

[4] Meakin, R.,"Computations of the Unsteady Flow About a Generic Wing/Pylon/Finned-Store Configuration," AIAA Paper 92-4568, Aug. 1992.

[5] Jameson, A., Baker, T. J., and Weatherhill, N. P., "Calculation of Inviscid Transonic Flow over a Complete Aircraft," AIAA Paper 86-0103, Jan. 1986.

[6] Peraire, J., Peiro, J., and Morgan, K., "A 3D Finite Element Multigrid Solver for the Euler Equations," AIAA Paper 92-0449, Jan. 1992.

[7] Löhner, R., and Baum, J. D., "Three-Dimensional Store Separation Using a Finite Element Solver and Adaptive Remeshing," AIAA Paper 91-0602, Jan. 1991.

[8] Frink, N. T., "Upwind Scheme for Solving the Euler Equations on Unstructured Tetrahedral Meshes," *AIAA Journal*, Vol. 30, No. 1, 1992, pp. 70–77.

[9] Frink, N. T., Parikh, P., and Pirzadeh, S., "A Fast Upwind Solver for the Euler Equations on Three-Dimensional Unstructured Meshes," AIAA Paper 91-0102, Jan. 1991.

[10] Frink, N. T., Parikh, P., and Pirzadeh, S., "Aerodynamic Analysis of Complex Configurations Using Unstructured Grids," AIAA Paper 91-3292, Sept. 1991.

[11] Parikh, P., Pirzadeh, S., and Löhner, R., "A Package for 3-D Unstructured Grid Generation, Finite-Element Flow Solutions, and Flow-Field Visualization," NASA CR-182090, Sept. 1990.

[12] Pirzadeh, S., "Recent Progress in Unstructured Grid Generation," AIAA Paper 92-0445, Jan. 1992.

[13] Heim, E. R., "CFD Wing/Pylon/Finned Store Mutual Interference Wind Tunnel Experiment," Arnold Engineering Development Center, AEDC-TSR-91-P4, Jan. 1991.

[14] Pirzadeh, S., "Structured Background Grids for Generation of Unstructured Grids by Advancing Front Method," *AIAA Journal*, Vol. 31, No. 2, 1993, pp. 257–265.

[15] Parikh, P., Pirzadeh, S., and Frink, N., "Unstructured Grid Solutions to a Wing/Pylon/Store Configuration Using VGRID3D/USM3D," AIAA Paper 92-4572, Aug. 1992.